Cold Plasma Diagnostics Using Satellite Measurements of VLF Signals From Ground Transmitters

U. S. INAN AND T. F. BELL

Radioscience Laboratory, Stanford University, Stanford, California 94305

R. R. ANDERSON

Department of Physics and Astronomy, University of Iowa, Iowa City, Iowa 52242

A new diagnostic technique to obtain the cold plasma density profile in the magnetosphere is introduced. This method uses satellite measurements of group delay and pulse duration of VLF signals from ground transmitters in conjunction with a detailed ray tracing analysis. An iterative method is involved. This method starts with an approximate density profile, computes the ray paths for that profile, and then compares the properties of the rays that reach the satellite location with the actual satellite measurements. The density profile is then modified to account for any discrepancies between the two results. The same process is repeated with the new profile until one has reasonable agreement between the data and ray tracing results. This method is applied to the case of an Imp 6 pass on June 28, 1973, where strong signals from the Siple VLF transmitter were observed for over 25 min. Good agreement is found between the results of the new technique and the well-known ground whistler techniques of cold plasma diagnostics. The results also serve to illustrate the wide diversity of paths of propagation from ground transmitters to high-altitude satellites during VLF wave injection experiments.

INTRODUCTION

The purpose of this paper is to report on a new diagnostic technique to obtain the cold plasma distribution in the magnetosphere. The idea is to use measurements of VLF signals from ground transmitters as they are received on high-altitude satellites. We show that accurate measurements of time delay and pulse duration of such signals combined with detailed ray tracing analysis allow the construction of the plasma density profile. It is even possible in some cases to identify small irregularities on the plasmapause. Our method is basically an iterative one. We start with three items: (1) a plot of pulse group time delay versus time, such as that shown in Figure 1, (2) a plot of pulse duration versus time, and (3) an assumed rough model of the magnetospheric equatorial cold plasma density, as shown in Figure 2.

The plasma density model represents a rough average density profile as determined through the well-known whistler technique of cold plasma diagnostics [*Carpenter and Smith*, 1964; *Angerami and Carpenter*, 1966; *Park*, 1972]. In keeping with the whistler technique it is assumed that a diffusive equilibrium model of electron density holds inside the plasmapause and that a collisionless model holds in the low-density region outside the plasmapause. The inside and outside branches are shown with solid lines in Figure 2. The portion shown with dashes is a region where a mixture of both models may apply. As the first step we hold the shapes of the solid line portions of Figure 2 constant while we normalize their amplitudes. This is done by computing the time delays from the ground to the satellite with a ray tracing analysis using the tentative model given in Figure 2. Two such computations must be done: (1) for a ray that reaches the satellite through a path that lies just inside the plasmapause and for which a diffusive equilibrium model for electron density is used and (2) for a ray that reaches the satellite through a path that lies entirely in the low-density region outside the plasmapause and for which a collisionless density model is used. These calculations are done with the Stanford VLF ray tracing program [*Burtis*, 1974]. The program automatically selects a diffusive equilibrium and collisionless model inside and outside the plasmapause, respectively. The group time delays from the ground to the satellite location for both rays are computed and compared with the measured time delays. The inside and outside density levels in Figure 2 are then scaled up or down according to the difference between the computed and the measured time delay values. (Note that the whistler mode group delay is proportional to the square root of the equatorial cold plasma density for both the diffusive equilibrium and the collisionless models.) The result of this adjustment is a working model of the plasma distribution such as that shown in Figure 3. The working model is then used in a ray tracing survey to compute all possible ray paths to the satellite during the time of observation. The calculated group time delays and pulse durations are then compared with the observed values of these quantities, and adjustments are made in the working model of the plasma density to reflect any differences between calculation and observation. The ray tracing survey is then repeated by using the corrected plasma density model, and any further differences between calculation and observation are used to correct this second model. The iteration proceeds until satisfactory agreement is reached between calculation and observation. To provide an example of this method, we now focus upon the VLF data acquired during an Imp 6 pass on June 28, 1973.

IMP 6 PASS ON JUNE 28, 1973

Our example is based on VLF broadband data received during the inbound pass of the Imp 6 satellite on June 28, 1973, at a time when the Siple Station transmitter in Antarctica was transmitting special programs for the satellite. This activity was part of a Stanford University–University of Iowa joint experiment in which VLF waves from the Siple Station transmitter were injected into the magnetosphere and detected near the magnetic equatorial plane by the Explorer 45 and Imp 6 spacecraft. The results from the initial 3-month period of this experiment are reported in a companion paper [*Inan et al.*, 1976], hereafter referred to as paper 1. In the present paper we focus attention on the Imp 6 pass on June 28, 1973, where

Paper number 6A0900.

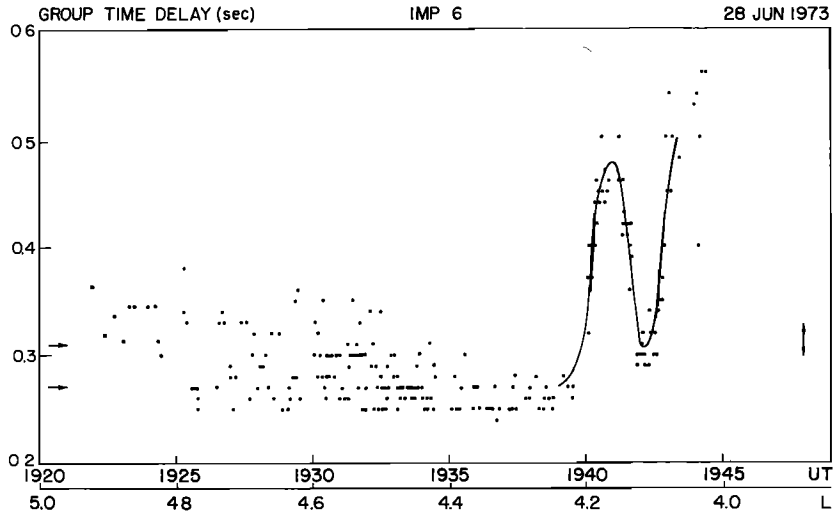

Fig. 1. The variation of group time delay of the Siple transmitter pulses as observed on Imp 6. The uncertainty in the measurements is indicated by a double arrow.

strong Siple signals were observed on the satellite continuously for over 25 min during the period 1920–1950 UT. The reader is referred to paper 1 for background information concerning the June 28 pass. (For instance, Figure 3 of paper 1 shows a portion of the Imp 6 orbit in a magnetic meridian plane projection, and the program of transmissions to the satellite and the reception on the satellite are discussed and shown in Figures 4 and 5 of paper 1.) In the following material we describe detailed measurements on the received signals and show how it is possible to use these measurements to construct the radial density profile.

Pulse Group Delay

The group delay associated with the higher-frequency (5.620 kHz) pulses was readily measurable throughout the entire period 1925–1950 UT. The measurements are given as a plot of group delay versus real time in Figure 1. Each dot in that figure represents an individual pulse. The estimated uncertainty due to measurement errors is indicated by the double arrow.

An important feature of the variation of time delay is the sharp increase in the group delay around 1940 UT. This increase is almost a factor of 2 and cannot be explained by measurement error. Rather, it indicates the possibility of a density increase by approximately a factor of 4. Since this increase takes place in less than 30 s, it is likely that the satellite has encountered the plasmapause at that time. The L value for the position of the satellite at 1940 UT is about $L = 4.2$, which is a common position for the noontime plasmapause.

It is also seen from Figure 1 that after about 1941 UT the time delay drops and then rises again to high values at about 1943 UT. This significant change cannot be accounted for by measurement error. Again, this decrease can be attributed to a density decrease just after crossing the plasmapause. Such irregular structure at the plasmapause boundary has been reported [*Chappell et al.*, 1970; *Carpenter and Miller*, 1976] and is not uncommon.

Note that another interesting feature of Figure 1 is the relatively wide spread in time delay values in the period 1925–1935 UT. This spread is 3–4 times larger than the estimated uncertainty in measurements. The consistency of these results implies that this effect is real and that there actually are two or more possible values for the time delay. This means that there are at least two distinct paths from the transmitter to the satellite, the time delay on each path being different. This type of multipath propagation has been reported previously

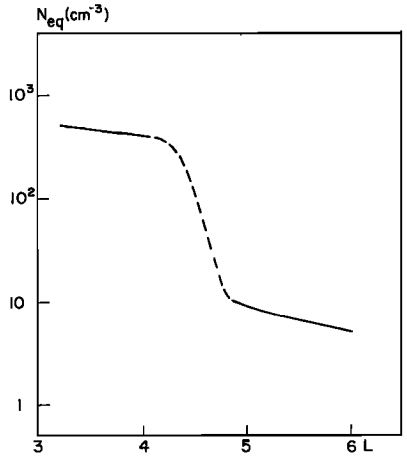

Fig. 2. An assumed rough model of the magnetospheric equatorial cold plasma density.

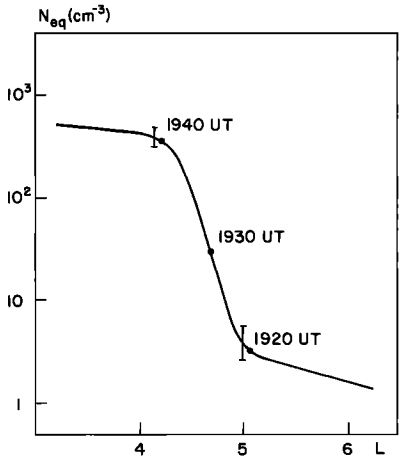

Fig. 3. The working model of the equatorial electron density. The error bars indicate the uncertainty in the inside and outside plasmapause density levels.

and is a common feature of nonducted propagation. The quick variations in time delay are presumably caused by rapid and selective fading that affects each path in a unique manner. This type of selective fading on multipath propagation has been reported previously. For instance, *Heyborne* [1966], using data from Ogo 1 and Ogo 2 satellites, reported that rapid and intense fading with as much as 20 dB suppression was possible in time spans of 1 s or less. *Scarabucci* [1969], using data from Ogo 4, concluded that upgoing waves near the plasmapause can experience deep amplitude fading. Furthermore, ground data from Roberval sometimes show the presence of deep and rapid fading of the Siple signal on ducted paths as well. The fading has been attributed to several factors, although the process is not fully understood. Large-scale ionization irregularities in the ionosphere and interference between two rays are possible causes.

The duration of the transmitter pulses was also measured throughout the same period. Both before and after the plasmapause crossing, pulse durations of 1.0 and 1.1 s were measured repeatedly and consecutively at the times when the transmitted pulse lengths were only 1 s. During the transmissions of the variable pulse length program, pulse lengths that were about 0.1 s larger than the transmitted lengths again were repeatedly observed. These observations are direct indications of the presence of more than one path from the ground to the satellite with time delays differing by as much as 0.1 s.

WORKING MODEL

Our aim now is to obtain an approximate plasma density profile using the gross features of the time delay variation. As is explained above, we use the rough model of Figure 2 to perform a ray tracing calculation for a ray inside and a ray outside the plasmapause. The calculated group time delays are then compared with the observed values of 0.45 ± 0.01 s inside the plasmapause at 1940–1942 UT and of 0.35 ± 0.01 s outside the plasmapause at 1920–1925 UT. By using the fact that the group time delay is proportional to the square root of the plasma density along the path the solid line portions of Figure 2 are adjusted to produce the working model of Figure 3. This working model now gives the appropriate time delay at 1940–1942 and 1920–1930 UT, but its prediction for other times is unknown. Furthermore, in constructing Figure 3 we have not used much of the other information that can be obtained from the time delay data, e.g., (1) the presence of multipath effects, (2) the time delays measured during 1925–1940 UT, and (3) the decrease in density around 1943 UT after the plasmapause crossing.

In order to improve further the profile of Figure 3 this profile is used to do a detailed ray tracing analysis involving a general survey of all possible ray paths to the satellite. The ray paths are computed by using the Stanford VLF ray tracing program written for the IBM 360/67 computer by *Walter* [1969] and improved by *Burtis* [1974]. The program performs ray tracing in a two-dimensional meridional plane using a centered dipole model for the magnetic field.

One of the main components of the input data to the ray tracing program is the field-aligned electron density model. By adjusting the various input parameters of the program it is possible to input a field-aligned electron density model whose equatorial profile is identical to that of Figure 3. The ionosphere is also simulated by appropriate vertical density gradients.

The wave input to the program consists of a value of frequency, wave normal, and location (invariant latitude and altitude) of the initial point. The waves are injected with vertical wave normals at 100-km initial altitude. The wave frequency used is the transmitted frequency of 5620 Hz. A survey was made by varying the initial ray injection latitude. Latitudes ranging from 52° to 63° were used.

Figure 4 shows the ray paths corresponding to ray injection latitudes in the range cited above. The position of the satellite for the time period 1920–1945 UT is also shown. For the rays reaching the satellite the group time delay from the ground to the satellite (Δt) is given. The dipole field line corresponding to $L = 4.15$ is shown by a dotted line. In our working model the $L = 4.15$ field line is the inward edge of the plasmapause. An example of a ray path shown in a geomagnetic field plot is given in Figure 7 of paper 1. The reader is referred to that figure for better comprehension of the format of Figure 4.

As is seen in Figure 4, the rays with initial latitudes in the range 54°–60° are trapped by the edge of the plasmapause. All of these rays cross the satellite location at more or less the same point and have almost equal group time delay. As initial ray injection latitude is increased above 60°, the ray paths 'curve in' at low altitudes to lower L shells mostly owing to the steep plasmapause gradients at low altitudes. This trend continues until about 61.4° initial latitude. When the initial latitude is further increased, the ray paths start to 'curve out' toward higher L shells. After further increase in injection latitude the ray paths lie almost completely outside of the steep plasmapause gradient. In this low-density region the rays generally diverge outward at all latitudes because of the slow (r^{-4}) density decrease.

The important features of the behavior of the ray paths, as pictured in Figure 4, are as follows, The satellite locations inside the $L = 4.15$ field line are illuminated by more than one possible ray path. The rays of one group that ends up in that region are those that are trapped by the edge of the plasmapause, i.e., the rays with 54°–60° initial latitudes. In addition, two more rays (one in the range 60°–61.4°, the other in the range 61.4°–61.8°) can also end up at a particular point on the satellite path inside the $L = 4.15$ field line. So for the satellite path after 1940 UT, more than one ray can reach the satellite at the same time. On the other hand, we see that before 1940 UT, each point on the satellite path is illuminated by only one ray coming from a specific initial latitude.

The group time delay observations cannot be entirely explained with the ray paths as described above. We have observed that both before and after 1940 UT the pulse duration is larger than that transmitted because of multipath propagation. However, the rays described above show that more than one path is not possible before 1940 UT. Thus the simple model cannot fully explain the data.

The measured time delay values for the period 1925–1940 UT vary from 0.27 to 0.33 s. The higher values compare well with the calculated values of 0.32–0.38 s. Hence the working model gives a reasonable first approximation. However, the model can be refined to better explain the observations.

CORRECTED MODEL

One of the main deficiencies of the working model is its inability to predict multipath propagation for L shells higher than 4.2. One method of producing more than one path in this region is introducing an irregularity in the radial density profile across the plasmapause. Such an irregularity is introduced at $L \sim 4.7$, as is shown in Figure 5.

The sharp increase in the time delay at 1940 UT was interpreted as the plasmapause crossing. By the same token, the

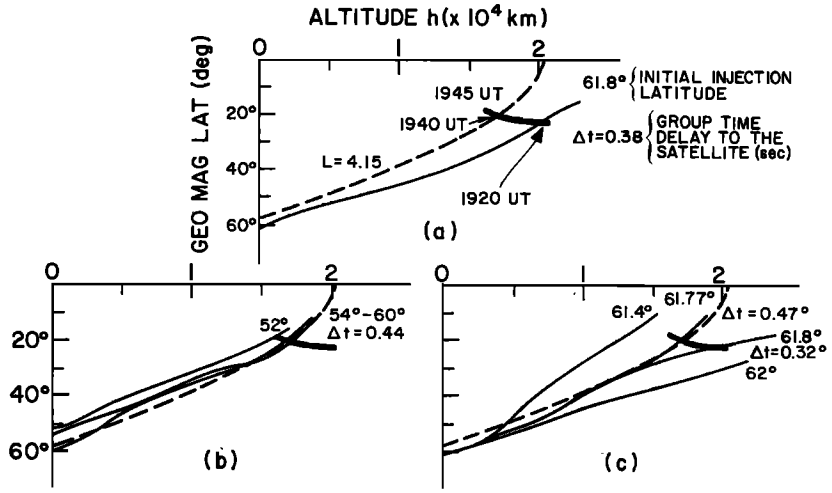

Fig. 4. Ray paths of 5.62-kHz waves obtained with the working model. The dotted line shows the $L = 4.15$ dipole field line, i.e., inward edge of the plasmapause. The thick solid line shows the satellite locations for the period 1920–1945 UT. (*a*) The description of the figure format. The $L = 4.15$ field line and satellite path are shown. The corresponding universal times for the satellite location are also shown. The number at the tip of each ray path shows the initial injection latitude at 100-km altitude. For the rays crossing the satellite path the group time delay from the ground to the satellite (Δt) is given in seconds. (*b*) Ray paths for injection latitudes 52°–62°. (*c*) Ray paths for injection latitudes larger than 60°.

decrease in time delay at around 1943 UT after the plasmapause crossing implies a density depression just inside the plasmapause around $L \sim 4.1$. Such a density decrease is shown in Figure 5. The profile given in Figure 5 thus represents a tentative corrected density profile. To be precise, Figure 5 differs from Figure 3 in that a density enhancement of width about $0.03L$ has been introduced at $L = 4.73$, and a 30% density depression of width about $0.2L$ has been introduced at $L = 4.12$. Previous observations of whistler ducts on satellites suggest that irregularities of this size may be common [*Angerami*, 1970].

To proceed with the iteration, a ray tracing survey using the corrected density model is now carried out in the same manner as that using the working model. Rays are injected at an altitude of 100 km with vertical wave normals, and a survey is made by varying the initial geomagnetic latitude from 52° to 63°. Figure 6 shows the ray paths corresponding to different ray injection latitudes. The format of this figure is the same as

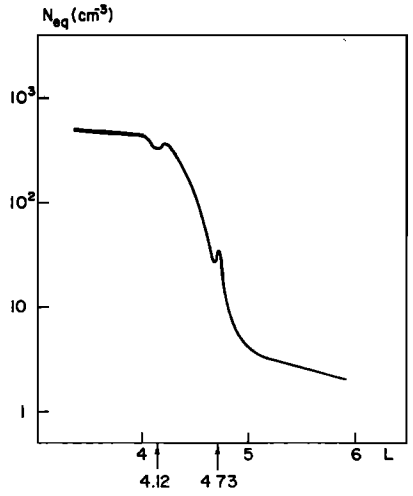

Fig. 5. Corrected model of the equatorial electron density. A 30% depression at $L = 4.12$ (width equals $0.26L$) and an enhancement by a factor of 2 at $L = 4.73$ (width equals $0.03L$) is introduced.

that of Figure 4. The detailed description of the different ray paths of Figure 6 is given in the appendix.

By taking account of the ray distribution of Figure 6 it can be shown that four to six separate rays will reach the satellite at each point in its orbit during the 1925–1940 UT period. This prediction is in agreement with our observations of multipath effects during this period.

The observed time delay versus real time curve given in Figure 1 shows that time delays of about 0.27 and about 0.33 s are consistently observed for the period 1925–1940 UT. For the corrected model the time delay values calculated are 0.21, 0.27, 0.37, and 0.46 s for the first four rays to intercept the satellite. The time delays of 0.37–0.46 s are somewhat higher than observed values in that region. However, these rays mostly travel on the plasmapause slope with L values between $L = 4.15$ and $L = 5.0$. By using lower-density values it is possible to obtain lower group delays, since the rays would then be propagating in a less dense medium. For the ray reaching the satellite with a time delay of 0.46 s a correction of about 25% is needed in order to obtain the measured time delay of about 0.33 s. Since the group delay is proportional to the square root of the electron density, this requires half as much density along the path of this ray. It should be noted from Figure 6*g* that this ray travels on the plasmapause slope while staying within L values of 4.2–5. A density profile that gives half as much electron density for $L = 4.2$–5 is shown with dotted lines in Figure 7. Such a profile yields time delay values that are in close agreement with the observations. Note that the 0.27-s time delay obtained for rays directed by the enhancement at $L = 4.73$ would not change, since the density at $L = 4.73$ is kept the same. The rays that are trapped at the foot of the plasmapause (see appendix) now illuminate a wider part of the satellite path, since the foot of the plasmapause is at lower L values for the profile given with dotted lines in Figure 7. Examples of such rays for the corrected model are shown in Figure 6*c*.

We now adopt the dotted line profile of Figure 7 as our new corrected model. Although further iterations can be performed to improve this model, we believe that we have demonstrated the method well enough to warrant stopping the iteration at

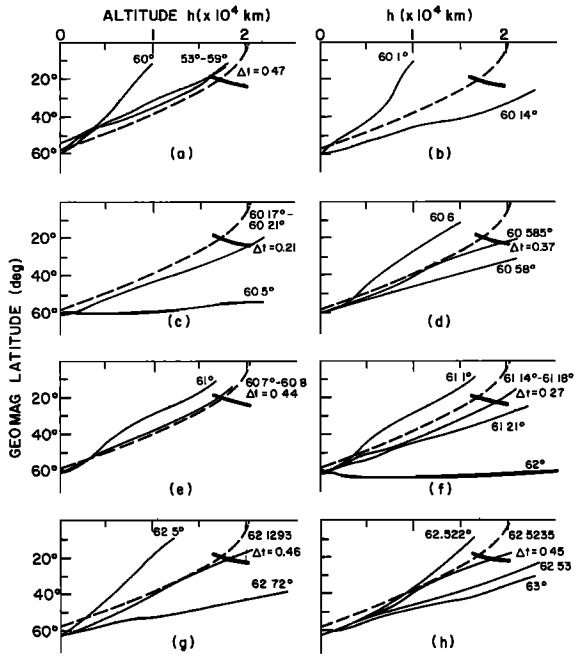

Fig. 6. Ray paths of 5.62-kHz waves obtained with the corrected model of the electron density. The format of this figure is exactly the same as that of Figure 4. The injection latitude is varied from 53° to 63°. Figures 6*a*–6*h* go in the order of increasing injection latitude.

this point. However, we do wish to point out the directions that further improvements might take. For example, the relatively low time delay of 0.27 s was observed throughout the period 1925–1940 UT. However, according to the results of the ray tracing analysis, which shows that rays that are ducted by the density enhancement at $L = 4.73$ (see Figure 6*f* and the appendix) exhibit time delays of 0.27 s, all such rays reach the satellite at more or less the same L value, i.e., $L = 4.73$. This L value on the satellite path corresponds to 1928 UT. The observation of short time delays in the 15-min period 1925–1940 UT can possibly be accounted for by leakage from the duct at $L = 4.73$. It should also be noted that the enhancement at $L = 4.73$ used for the corrected model has a relatively narrow spread in L. However, by using a wider enhancement it may be possible to explain directly the observation of short time delays over larger periods. (Observation of low time delays in the first section of the satellite path is explained by rays such as those shown in Figure 6*c*, which reach the satellite with time delays as low as 0.21 s.)

Another feature of the time delay variation that must be explained is the large decrease at 1942 UT. Our initial suggestion was that this decrease might be due to an electron density variation such as that given by the 30% density depression at $L = 4.12$, which was used in the corrected model. However, ray analysis has shown that further modification of the density profile is necessary to explain this observation. The problem here is the defocusing effect illustrated in Figure 6*b*. Since the wave frequency is below one half the local gyrofrequency, the rays do not propagate for long in the density depression. One way of keeping the rays in the low-density region, hence obtaining the low time delays seen at 1942 UT, is to have a relatively small enhancement of electron density at the center of the density depression.

It should be pointed out that the two density models plotted in Figure 7 have somewhat different gradient distributions across the plasmapause. Thus the ray paths for the dotted line distribution will differ slightly from those shown in Figure 6. Although the general behavior of the ray paths and the multipath effect will be the same and although our general conclusions will not be significantly affected, some applications may nevertheless require that further iterations be performed.

Multichannel Spectrum Analyzer Data

It is of interest to consider the conclusions drawn from the time delay and pulse duration data in light of several other types of independent measurements that can be used to obtain information about the cold plasma density. These measurements were all made by using the Imp 6 multichannel spectrum analyzers. Figure 8 shows the variation of the ratio cB_y/E_x for the 5.62-kHz channel as the satellite moves inward. Here, B_y and E_x are components of the wave electric and magnetic field that are orthogonal to each other as well as to the spin axis of the satellite. Clearly, this quantity does not have any particular significance unless the wave normal angle is known too. However, for longitudinal waves, i.e., waves that propagate along the static magnetic field, the ratio cB_y/E_x is proportional to the refractive index, which in turn is proportional to the square root of the cold plasma density. Hence for longitudinal waves

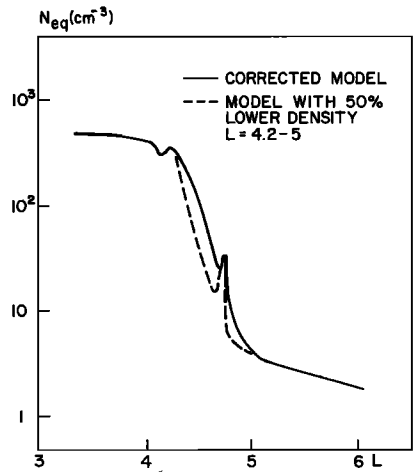

Fig. 7. Comparison of the corrected model used for ray tracing calculations and a model with 50% lower density values for $L = 4.2$–5.

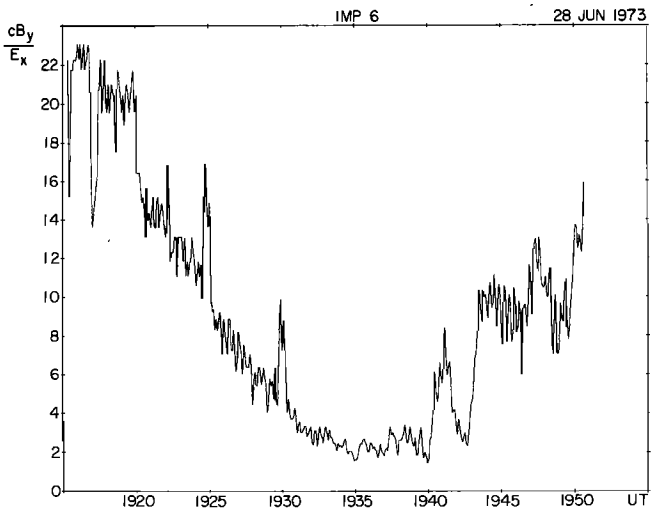

Fig. 8. The quantity cB_y/E_x versus time. Note that for field-aligned propagation, cB_y/E_x is proportional to the refractive index.

the group time delay (which is also proportional to the square root of plasma density) and the cB_y/E_x ratio should be proportional to each other. Our ray path computations have shown that the rays that reach the satellite after about 1930 UT are very nearly longitudinal. This is mainly due to the guiding effect of the large plasmapause gradient that tends to keep the wave normal aligned with the static magnetic field [*Inan and Bell*, 1976]. Before 1930 UT the rays reaching the satellite have higher wave normal angles. Comparing Figures 1 and 8 for the time period after 1930 UT, we see that the two results are in very good agreement. Namely, the variations of the group time delay and the cB_y/E_x ratio (for longitudinal propagation), both quantities that are proportional to the square root of cold plasma density, indicate a sharp density increase at 1940 UT (plasmapause encounter) and a subsequent density depression just inside the plasmapause.

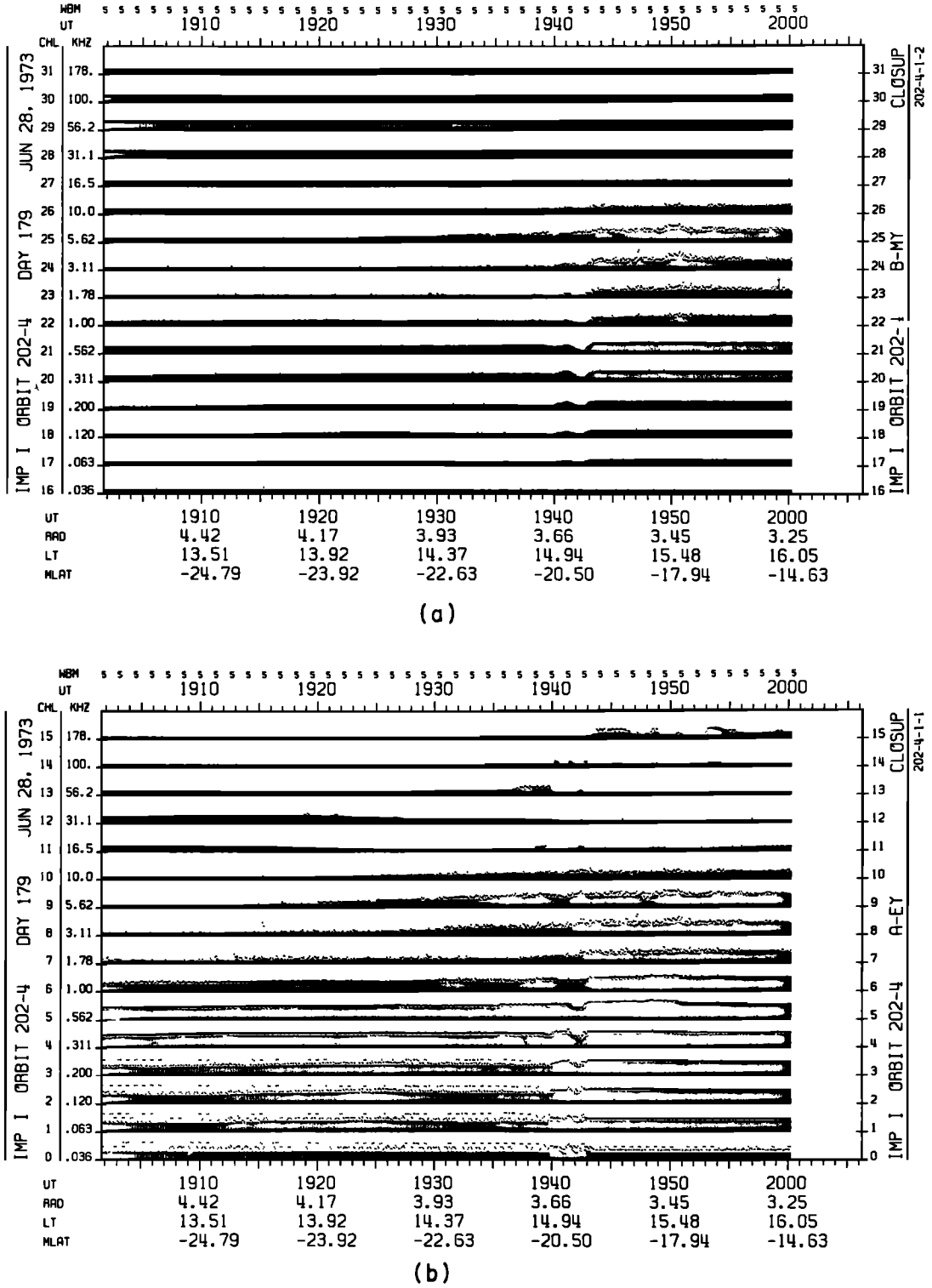

Fig. 9. Multichannel spectrum analyzer data from June 28, 1973, pass of Imp 6. (*a*) Data from magnetic antenna filter channel. (*b*) Data from electric antenna filter.

It should be noted at this point that although the two results are generally in good agreement, there are some important differences. For instance, as one of the reviewers has pointed out, the ratio of group delays at 1941 and 1943 UT is smaller than the ratio of the quantities cB_y/E_x taken at the same times. This can be explained by the fact that the group delay is a measure of the density integrated along the ray path whereas cB_y/E_x is a local parameter that measures local density.

Other aspects of the multichannel analyzer data also corroborate the above conclusions. Figure 9 shows a portion of the spectrum analyzer data from the June 28 pass, recorded as the satellite moves inward from about $L = 5.2$ to $L = 3.6$ and from a magnetic latitude of $-24.79°$ to $-17.94°$, respectively. The data shown are the raw voltage outputs of the two spectrum analyzers (proportional to the logarithm of signal amplitude), one connected to the E_x electric dipole and the other to the M_y magnetic loop antenna. The dynamic range of each frequency channel (100 dB) is represented by the distance from the base line of one channel to the base line of the next channel. Each vertical bar represents the time average electric (or magnetic) field strength measured over a time interval of 81.8 s, and the dots immediately above each bar represent the peak field strength seen over the same time interval.

In the magnetic antenna filter output data of Figure 9*a* a strong hiss band is observed to increase abruptly at 1940 UT and to cover the frequency range of about 200 Hz to 3 kHz. This plasmaspheric hiss is confined to the plasmasphere and is not seen outside the plasmapause [*Russell et al.*, 1969; *Russell and Holzer*, 1970; *Thorne et al.*, 1973]. Plasmaspheric hiss is observed on most Imp 6 passes through the plasmasphere, and the sudden emergence (inward passes) or termination (outward passes) of this hiss has been used as an indication of plasmapause crossing [*Shaw and Gurnett*, 1975].

Furthermore, note that in almost all channels where hiss is observed there is a significant dip in the signal intensity (following the increase at the plasmapause encounter at 1940 UT) for about 2–3 min around 1942 UT. This decrease in hiss intensity is seen to occur at the same time as the decreases in the time delay and the cB_y/E_x ratio. Plasmaspheric hiss is thought to be generated in a restricted L range just within the plasmapause, with waves subsequently propagating on complex paths to fill the plasmasphere [*Thorne et al.*, 1973; *Muzzio*, 1971]. If there is a density depression just inside the plasmapause, the waves will tend to be defocused away from the depressed region. Hence the observation of the decrease in the hiss signal intensity supports our interpretation of the group time delay data.

We now consider the electric antenna filter channel data given in Figure 9*b*. Information about the density structure encountered by the satellite can be obtained from the electrostatic noise bands observed at the high-frequency channels. The center frequency of the noise band increases systematically from 16.5 to 178 kHz as the satellite moves inward. At the plasmapause crossing at 1940 UT there is an abrupt increase from 56.2 to 100 kHz. Note that no corresponding signals are observed in the magnetic loop antenna data. Such electrostatic noise bands have been frequently seen on Imp 6 passes through the magnetosphere, and their center frequencies are associated with the electron plasma frequency [*Shaw and Gurnett*, 1975]. The center frequencies of 16.5 and 178 kHz correspond to number densities of about 3.3 and 390 cm^{-3}, respectively. These density values are typical of those measured outside and inside the plasmapause [*Angerami and Carpenter*, 1966]. Careful examination of the 56.2- and 100-kHz channels shows that after 1940 UT the noise band in these channels reappears and then disappears again. This again suggests an irregular structure just inside the plasmapause. It is evident that the number density abruptly rises to about 123 cm^{-3} (100 kHz) at the plasmapause encounter, then drops to about 39 cm^{-3} (56.2 kHz), and then rises back to and stays near 390 cm^{-3} (178 kHz) after about 1943 UT.

Thus three independent pieces of data corroborate the plasmapause crossing at 1940 UT and the density depression just inside the plasmapause around 1943 UT. Both of these effects were first diagnosed from the time delay measurements.

GROUND WHISTLER DENSITY PROFILE

We now compare the corrected profile given in Figure 7 with a density profile obtained by using the ground whistler technique. Continuous passive broadband (0–11 kHz) VLF recordings from Siple Station were analyzed for the periods 1820–1920 and 2020–2150 UT. These are periods just before and after the period of transmission to Imp 6 (1920–1950 UT) on June 28, 1973. Frequency time spectrograms covering these periods were analyzed to obtain whistler dispersion properties. Careful observation of events from both before and after the transmission period showed that there had not been significant movement of the whistler ducts in this 3-hour period.

Multiwhistler events were scaled for measurements of nose frequency and time delay. These values were then used together with appropriate magnetospheric models [see *Park*, 1972] to obtain a profile for radial variation of equatorial electron density n_{eq}. Figure 10 shows the profile from the ground data and the first and second corrected models. Figure 10 illustrates that both corrected profiles are in very good agreement with the density model from ground data.

Additional features of the Imp 6 data were the multihop whistler events that were observed after about 1942 UT. One such event is shown in Figure 11. The multihop property of this event shows that it is somehow ducted. Many such events were observed for over 6 min, or over a distance of about 800 km. This distance is much larger than common duct dimensions [*Angerami*, 1970]. It is known [*Helliwell*, 1965] that VLF waves can be trapped on the inner edge of steep gradients of electron density. The existence of trapped modes due to plasmapause gradients was first predicted theoretically by F. Walter (unpublished papers, 1969). The properties of such guidance by plasmapause gradients have recently been studied

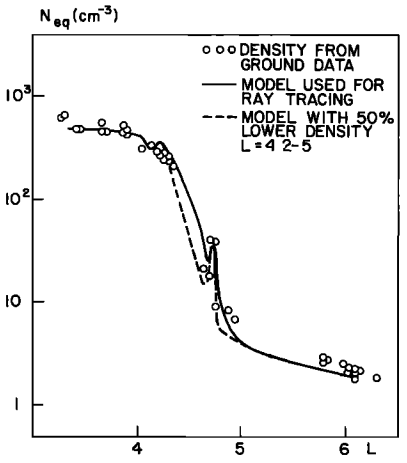

Fig. 10. Comparison of the density profile obtained from ground whistler analysis with the first and second corrected models.

[*Inan and Bell*, 1976]. In the case shown in Figure 11 it was found that guiding was provided by the inner edge of the density depression just inside the plasmapause.

It was also found that the two-hop time delays observed for the multihop whistlers given in Figure 11 were in agreement with the prediction of our corrected model. Furthermore, it was found that rays coming from a latitude range of about 5° in the southern (northern) hemisphere with vertical wave normal angles will propagate to their conjugate points and arrive there with vertical wave normals also. These paths are quasi-reciprocal, and waves can be specularly reflected from the lower end of each ionosphere and bounce back and forth between hemispheres. This type of propagation is possible over a wide frequency range (1–5 kHz) [*Inan and Bell*, 1976].

Summary and Conclusions

We have shown that satellite measurements of VLF signals from ground transmitters can be used as a diagnostic tool to study the magnetosphere. We have demonstrated that with the aid of a ray tracing analysis the time delay and pulse duration characteristics of the transmitter signals can be used to obtain the cold plasma density profile. The density profile obtained was found to be in good agreement with that obtained from the ground whistler technique. We have also shown that other independent data from the multichannel spectrum analyzer on the satellite corroborated our findings.

Although previous attempts have been made to use satellite observations of ducted natural whistlers as diagnostic tools [*Smith and Angerami*, 1968], to our knowledge this is the first report of cold plasma diagnostics with the aid of high-altitude satellite measurements of nonducted signals from ground transmitters.

It is important to point out here that in the past a number of authors have used low-altitude satellite measurements to infer the density structure in the topside ionosphere [*Aubry*, 1967, 1968; *James*, 1972; *Malingre*, 1973; *Cerisier*, 1973, 1974; and *Edgar*, 1976] by using field intensity and Doppler shift measurements. In addition, *Edgar* [1976] was able to infer equatorial density structure below $L \sim 3$ from the FR 1 and Isis 2 low-altitude Doppler data.

Our work differs from past work in that we have used time delay measurements from a high-altitude satellite to infer the density structure at higher altitudes (20,000–30,000 km). The Doppler shift diagnostic technique used by past workers does not in general appear appropriate for high-altitude satellite work. This comes about because signal reception at high altitude ($L > 3$) does not generally take place via the MR (magnetospherically reflected) mode [*Edgar*, 1972], and thus the wave refractive index at the satellite location is generally much smaller than the wave refractive index at low altitude (in the hemisphere conjugate to the transmitter). Furthermore, the high-altitude satellite velocity is smaller than the velocity of the low-altitude satellite. These two differences cause the Doppler shifts measured by high-altitude satellites to be much smaller than the Doppler shifts measured by low-altitude satellites.

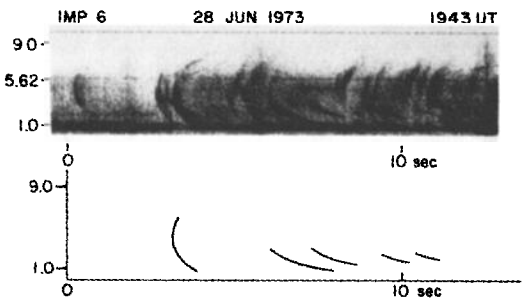

Fig. 11. An example of the multihop whistler events observed after 1941 UT.

As a case in point we calculate on the basis of our ray tracing analysis that the maximum Doppler shift associated with the Imp 6 receptions on June 28, 1973, was approximately 5 Hz. This can be compared with the Doppler shifts of 100–200 Hz measured on the low-altitude satellites FR 1 and Isis 2 [*Edgar*, 1976]. Although a Doppler shift of 5 Hz can in principle be measured, it is not a simple task in practice. Furthermore, there are a number of effects that will tend to mask this small Doppler shift. For instance, the spectral broadening of monochromatic pulses due to nonlinear amplification is also of the order of 5–10 Hz [*Stiles and Helliwell*, 1975], and the Doppler shift due to electric field induced cross L plasma flow can also be as large as 5 Hz. Thus the difficulties in the Doppler technique appear to make the time delay technique better suited to high-altitude satellite measurements.

It is instructive to compare our method to the ground whistler method of magnetospheric diagnostics. In the whistler method the time delay and nose frequency measurements of ducted whistlers are used in conjunction with assumed density models in order to obtain the equatorial cold plasma density profile [*Carpenter and Smith*, 1964; *Angerami and Carpenter*, 1966; *Park*, 1972]. In our own method, time delay and pulse duration measurements of fixed frequency nonducted pulses from a VLF ground transmitter are used in conjunction with ray tracing techniques and assumed density models to obtain the equatorial cold plasma density profile. While our method is more complex than the whistler method, in principle it should yield more information concerning the plasma distribution. This comes about because of the fact that a nonducted wave generally samples density over a wide range of L shells, while a ducted wave samples density only on a particular L shell. At present we can say little about the uniqueness of the plasma profiles produced by our method. This important question is still under investigation. However, it is clear that the results obtained by using our method will be valid only insofar as the diffusive equilibrium and collisionless density models are valid.

This new diagnostic method could be further extended. With the satellite measurement of wave normals and with the usage of more carefully designed transmission programs (e.g., frequency ramps instead of pulses would make the multipath effects more readily noticeable) it should be possible to determine the cold plasma density much more efficiently and precisely than we have done here. However, the satellite measurement of wave normals can be difficult when two or more waves are present at once.

The study reported in this paper has also produced some important results that are used in the companion paper [*Inan et al.*, 1976], referred to as paper 1. The following are the findings that are relevant to the discussion in paper 1.

1. The pulses in Figure 6*c* of paper 1 reached the satellite by direct paths between transmitter and satellite. It was not possible for the pulses to reach the satellite in the MR (magnetospherically reflected) mode [*Edgar*, 1972] after being reflected once in the northern hemisphere.

2. The time delay of the pulses from transmitter to satellite varied from 0.27 s on the shortest path to 0.37 s on the longest path.

3. The emissions of Figure 6*c* of paper 1 were detected at 1938 UT, at which time the satellite was in a low plasma density region just outside the plasmapause.

Apart from the above conclusions and findings our analysis has also demonstrated the diversity of paths of signal propagation from ground transmitters to high-altitude satellites. We believe that much remains to be learned about both ducted and nonducted magnetospheric wave propagation through further studies of satellite-supported VLF wave injection experiments.

APPENDIX: DESCRIPTION OF THE RAY PATHS OF FIGURE 6

The computed ray paths for the corrected model given in Figure 5 are shown in Figure 6. In this appendix we give a detailed description of the ray distribution. We discuss the ray paths in the order of increasing initial injection latitude.

The rays injected from initial latitudes 53°–59° are gradient trapped by the negative density gradient provided by the 30% density depression at $L = 4.12$. Examples of these are shown in Figure 6*a*. The propagation of these rays is very similar to the rays obtained by using the working model density profile for initial latitudes 54°–60°, as given in Figure 4*b*. Those rays were gradient trapped by the inner edge of the plasmapause. The major difference between the rays given in Figure 4*b* and Figure 6*a* is that in the latter case the ray paths are limited to lower L values, since the density depression that acts as the trapping gradient is at a lower L shell.

As the initial latitude is increased, the ray paths bend in, as is shown in Figure 6*a* for the path for a ray injected at 60°. These rays start on the decreasing edge of the density depression at $L = 4.12$ and are sharply bent inward by this gradient. The ray injected at 60.1°, shown in Figure 6*b*, is also in this category. The ray starting at 60.14°, on the other hand, starts on the increasing edge of the density depression and is bent sharply outward. This is the well-known defocusing effect for whistler mode propagation in a depression of ionization for frequencies less than half the gyrofrequency [*Helliwell*, 1965].

We now consider Figure 6*c*. The rays with initial latitude 60.17°–60.21° start at the increasing edge of the density depression and are bent outward at low altitudes. However, these rays are then trapped and guided by the trough at the foot of the plasmapause. This mode of guiding has been discussed by *Inan and Bell* [1976]. These rays propagate in an almost field aligned mode, and their L values stay within $L = 4.8$ and $L = 5.0$. As is indicated in Figure 6*c*, such rays reach the satellite with quite low time delays. As initial latitude is further increased, the rays diverge outward.

Figure 6*d* shows ray paths for initial latitudes 60.58°–60.6°. As initial latitude is increased from 60.5°, the rays rapidly bend inward. The ray starting at 60.6° bends in to lower L values at low altitudes and does not reach the satellite.

Rays with initial latitudes 60.7°–60.8° also bend in at low altitudes, but these rays are trapped and guided by the density enhancement formed between the 30% density depression at $L = 4.12$ and the plasmapause. This is the usual two-sided ducted mode propagation. These rays are shown in Figure 6*e*.

Further increase in the initial injection latitude results in rays that again bend in at low altitudes. The ray starting at 61° is an example of this. After about 61.1° initial latitude the ray paths start to bend out.

The rays injected from the latitude range 61.14°–61.19° are quite special. These rays are trapped and ducted by the density enhancement at $L = 4.73$. They travel with ray angles very close to zero and hence almost parallel to the magnetic field line. For this reason they have a high group velocity and arrive at the satellite with a time delay of about 0.27 s. Since they are ducted, all rays from latitudes 61.14°–61.19° reach the satellite at almost the same point.

Further increase in initial latitude results in rays that quickly diverge out, as is seen in the figure. The ray injected at 62.0° propagates to L values larger than 10 before it reaches 10,000-km altitude. But this particular ray is approximately the outermost one. That is, when initial latitude is further increased, the ray paths again bend inward. The ray injected at 62.5° ends up at very low L values, as is seen in the figure. This great difference between rays injected at 62.0° and 62.5° is caused by the presence of the density enhancement at $L = 4.73$. This L value corresponds to a latitude of 62.25° at injection altitude of 100 km. Hence rays injected at 62.0° and 62.5° start at L values lower and higher than that of the duct, respectively. Hence they have quite different ray paths. It should be noted that the rays reaching the satellite in Figure 6*g* are not trapped in the duct.

As the initial injection latitude is further increased, the rays diverge out. These rays are not affected by the presence of the irregularities. They start at higher L values. For latitudes between 62.5° and 62.53° the rays tend to follow the curvature of the field lines, guided by the gradients at the outer edge of the plasmapause, but as initial latitude is increased, they are no longer guided, diverge outward, and do not reach the satellite.

Acknowledgments. We wish to acknowledge the many valuable discussions we have held with our colleagues at both the Radioscience Laboratory at Stanford University and the Department of Physics and Astronomy at the University of Iowa. Special thanks are due to D. L. Carpenter for his help in preparing the ground whistler density profile of Figure 10. The research work of two of us (U.I. and T.B.) was supported by the National Aeronautics and Space Administration under grant NGL-05-020-008. The work of the remaining author (R.A.) was supported by the National Aeronautics and Space Administration under contract NAS5-11167 and grant NGL-16-001-043 and by the Office of Naval Research.

The Editor thanks J. C. Cerisier and H. C. Koons for their assistance in evaluating this paper.

REFERENCES

Angerami, J. J., Whistler duct properties deduced from VLF observations made with the Ogo 3 satellite near the magnetic equator, *J. Geophys. Res., 75*, 6115, 1970.

Angerami, J. J., and D. L. Carpenter, Whistler studies of the plasmapause in the magnetosphere, 2, Electron density and total tube content near the knee in the magnetospheric ionization, *J. Geophys. Res., 77*, 711, 1966.

Aubry, M. P., Influence des gradients horizontaux de densité électronique sur la direction des normal d'ondes TBF dans l'ionosphère, *Ann. Geophys., 23*, 467, 1967.

Aubry, M. P., Some results of the FR-1 satellite experiment on the VLF wave field in the zone close to the transmitter, *J. Atmos. Terr. Phys., 30*, 1161, 1968.

Burtis, W. J., Users' guide to Stanford VLF raytracing program, Radioscience Lab., Stanford Elec. Lab., Stanford Univ., Stanford, Calif., 1974.

Carpenter, D. L., and T. R. Miller, Ducted magnetospheric propagation of signals from the Siple, Antarctica, VLF transmitter, *J. Geophys. Res., 81*, 2692, 1976.

Carpenter, D. L., and R. L. Smith, Whistler measurements of electron density in the magnetosphere, *Rev. Geophys Space Phys., 2*, 415, 1964.

Cerisier, J. C., A theoretical and experimental study of non-ducted VLF waves after propagation through the magnetosphere, *J. Atmos. Terr. Phys., 35*, 77, 1973.

Cerisier, J. C., Ducted and partly ducted propagation of VLF waves through the magnetosphere, *J. Atmos. Terr. Phys., 36*, 1443, 1974.

Chappell, C. R., K. K. Harris, and G. W. Sharp, A study of the

influence of magnetic activity on the location of the plasmapause as measured by Ogo 5, *J. Geophys. Res., 75,* 50, 1970.

Edgar, B. C., The structure of the magnetosphere as deduced from magnetospherically reflected whistlers, *Tech. Rep. 3438-2,* Radioscience Lab., Stanford Elec. Lab., Stanford Univ., Stanford, Calif., 1972.

Edgar, B. C., The theory of VLF Doppler signatures and their relation to magnetospheric density structure, *J. Geophys. Res., 81,* 3327, 1976.

Helliwell, R. A., *Whistlers and Related Ionospheric Phenomena,* Stanford University Press, Stanford, Calif., 1965.

Heyborne, R. L., Observations of whistler-mode signals in the Ogo satellites from VLF ground station transmitters, *Tech. Rep. 3415/3418-1,* Radioscience Lab., Stanford Elec. Lab., Stanford Univ., Stanford, Calif., 1966.

Inan, U. S., and T. F. Bell, The plasmapause as a VLF wave guide, submitted to *J. Geophys. Res.,* 1976.

Inan, U. S., T. F. Bell, D. L. Carpenter, and R. A. Anderson, Explorer 45 and Imp 6 observations in the magnetosphere of injected waves from the Siple Station VLF transmitter, *J. Geophys. Res., 82,* this issue, 1977.

James, H. G., Refraction of whistler-mode waves by large scale gradients in the middle-latitude ionosphere, *Ann. Geophys., 28,* 301, 1972.

Malingre, M., Défocalisation des ondes TBF dans l'ionosphère supérieure au voisinage de la dépression de moyenne latitude, *Ann. Geophys., 29,* 239, 1973.

Muzzio, J. L. R., ELF propagation in the plasmasphere based on satellite observations of discrete and continuous forms, *Tech. Rep. 3439-2,* Radioscience Lab., Stanford Elec. Lab., Stanford Univ., Stanford, Calif., 1971.

Park, C. G., Methods of determining electron concentrations in the magnetosphere from nose whistlers, *Tech. Rep. 3454-1,* Radioscience Lab., Stanford Elec. Lab., Stanford Univ., Stanford, Calif., 1972.

Russell, C. T., and R. E. Holzer, AC magnetic fields, in *Particles and Fields in the Magnetosphere,* D. Reidel, Dordrecht, Netherlands, 1970.

Russell, C. T., R. E. Holzer, and E. J. Smith, Ogo 3 observations of ELF noise in the magnetosphere, 1, Spatial extent and frequency of occurrence, *J. Geophys. Res., 74,* 755, 1969.

Scarabucci, R. R., Interpretation of VLF signals observed on the Ogo-4 satellite, *Tech. Rep. 3418-2,* Radioscience Lab., Stanford Elec. Lab., Stanford Univ., Stanford, Calif., 1969.

Shaw, R. R., and D. A. Gurnett, Electrostatic noise bands associated with the electron gyrofrequency and plasma frequency in the outer magnetosphere, *J. Geophys. Res., 80,* 4259, 1975.

Smith, R. L., and J. J. Angerami, Magnetospheric properties deduced from Ogo 1 observations of ducted and nonducted whistlers, *J. Geophys. Res., 73,* 1, 1968.

Stiles, G. S., and R. A. Helliwell, Frequency-time behavior of artificially stimulated VLF emissions, *J. Geophys. Res., 80,* 608, 1975.

Thorne, R. M., E. J. Smith, R. K. Burton, and R. E. Holzer, Plasmaspheric hiss, *J. Geophys. Res., 78,* 1581, 1973.

Walter, F., Nonducted VLF propagation in the magnetosphere, *Tech. Rep. 3418-1,* Radioscience Lab., Stanford Elec. Lab., Stanford Univ., Stanford, Calif., 1969.

(Received July 23, 1976;
accepted November 26, 1976.)